J Mater Sci (2009) 44:2647–2655
DOI 10.1007/s10853-009-3346-6

Achieving high strain rate superplasticity in cast 7075Al alloy via friction stir processing

F. C. Liu · Z. Y. Ma

Received: 4 September 2008 / Accepted: 13 February 2009 / Published online: 9 March 2009

Abstract Cast 7075Al alloys under as-cast and homogenized conditions were subjected to single-pass friction stir processing (FSP). FSP converted the coarse as-cast structure to the fine-grained structure with a grain size of 2.5–3.2 μm. A pre-homogenization prior to FSP was beneficial to the generation of a more uniform microstructure in the FSP sample with smaller particles and grains. Both FSP samples exhibited high strain rate superplasticity at 1×10^{-2} s^{-1} and 450 °C. Cavitation developed at the particles and the grain triple junctions. The superplasticity of the FSP sample was significantly improved by the pre-homogenization prior to FSP, with a maximum superplasticity of 890% being observed, due to reduced particle size. The analyses of the superplastic data and scanning electronic microscopic (SEM) examinations indicated that grain boundary sliding is the main deformation mechanism for the FSP 7075Al.

Introduction

Superplastic deformation refers to the ability of materials to exhibit high uniform elongation when pulled in tension while maintaining a stable microstructure. There are two major prerequisites for achieving structural superplasticity. The first is a fine grain size, typically less than 10 μm. The second is thermal stability of the fine microstructure at high temperatures. Superplastic forming (SPF) is a well-established industrial process for the fabrication of complex shapes in sheet metals [1]. In practice, however, the use of SPF is generally limited to low volumes of components because there are two main factors restricting the commercial applications of SPF. First, the production of superplastic aluminum alloys is relatively expensive due to the complex thermomechanical processing (TMP) typically necessary to make these materials superplastic [2]. Second, the total forming time for a component is conventionally very long (up to ~30 min) due to the fact that the alloy exhibits superplastic behavior at a low strain rate ($<10^{-3}$ s^{-1}). As a result, the cost of the SPF production method can be prohibitive for high-volume production. To advance SPF into production oriented industries, there is a need to develop new easy and inexpensive processing techniques to shift the optimum superplastic strain rate to high value ($\geq 1 \times 10^{-2}$ s^{-1}).

FSP, a development based on friction stir welding (FSW) [3, 4], is a new solid state processing technique for microstructural modification [5, 6]. During FSP, the combination of large plastic deformation and thermal exposure results in the generation of fine recrystallized grains and the break-up of large particles. Thus, FSP creates a fine-grained microstructure with dispersively distributed particles and predominant high-angle grain boundaries, features that are important for enhanced superplastic properties.

The effects of FSP on the microstructure and superplastic properties of aluminum alloys have been widely studied [6–10]. Mishra et al. [6] reported the first result of the superplasticity of aluminum alloys using FSP. In their study, the optimum superplastic strain rate was 1×10^{-2} s^{-1} at 490 °C for the FSP 7075Al alloy with an average grain size of 3.3 μm. A succedent study by Ma et al. [7] showed that FSP 7075Al alloy with a grain size of 3.8 μm exhibited superplastic elongations of >1250% at

F. C. Liu · Z. Y. Ma (✉)
Shenyang National Laboratory for Materials Science,
Institute of Metal Research, Chinese Academy of Sciences,
72 Wenhua Road, Shenyang 110016, China
e-mail: zyma@imr.ac.cn

480 °C in the strain-rate range of 3×10^{-3}–3×10^{-2} s^{-1}. The optimum strain rate for the FSP 7075Al alloy is more than one order of magnitude higher than the previous best TMP effort on a 7075 aluminum alloy [6]. Recently, Johannes et al. [10] have successfully extended the effectiveness of FSP in creating larger areas of fine-grained aluminum alloy with superplastic properties by multiple pass FSP.

It should be pointed out that all the above mentioned superplastic investigations on the FSP 7075Al alloy were conducted using rolled plates as the raw materials for FSP. The commercial 7075 rolled plates are fabricated by the standard routes including homogenization, hot and cold rolling, and then special solution and aging treatments. For superplastic forming production, the main aim is to improve the structural performance of the workpiece and reduce the fabrication cost. If as-cast aluminum alloys are directly used as the raw materials to produce fine-grained structure via FSP, it will significantly shorten the fabrication period of superplastic materials and reduce the fabrication cost. Several previous studies have shown that FSP can result in significantly enhanced superplasticity in as-cast A356, 5083, and Al–Zn–Mg–Sc aluminum alloys [11–13]. However, no study on FSP of the castings of high-strength commercial aluminum alloys is reported so far. Therefore, it is of practical importance to conduct FSP on the 7075Al casting to produce the fine-grained structure. In this study, cast 7075Al alloy was subjected to FSP and superplastic investigation. The aim is (a) to examine the possibility of achieving superplasticity in cast 7075Al via FSP and (b) to evaluate the effect of initial structure on superplasticity.

Experimental

Cast 7075Al alloy with a nominal composition of 5.85Zn–2.56Mg–1.89Cu–0.22Cr (in wt%) was used as raw material. Plates of $8 \times 100 \times 300$ mm^3 were cut from the casting. While one plate was directly friction stir processed (denoted as D-FSP), the other plate was subjected to a homogenization treatment before FSP (denoted as H-FSP). The homogenization was conducted at 462 °C for 24 h, and then the temperature was increased to 470 °C at a rate of 0.5 °C/h followed by water cooling. FSP was conducted at a tool rotation rate of 1200 rpm and a traverse speed of 100 mm/min. The total FSP length was around 270 mm from the pin entry to the pin exit. A tool with a concave shoulder 16 mm in diameter, and a threaded conical pin 5 mm in root diameter, 3.5 mm in tip diameter, and 4.5 mm in length was used.

Microstructure characterization was performed on the cross-section of the stir zone (SZ) transverse to the FSP direction by optical and transmission electron microscope (OM and TEM). Grain sizes were measured by the mean linear intercept technique. Thin foils for TEM were prepared by twin-jet polishing using a solution of 70% methanol and 30% nitric acid at −35 °C and 19 V. To evaluate the superplastic behavior of the FSP samples, dog-bone shaped tensile specimens (3 mm gage length, 1.5 mm gage width and 1.0 mm gage thickness) were electro-discharge machined from the transverse cross-section of the stir zone (SZ). These specimens were subsequently ground and polished to a final thickness of ~0.8 mm. Constant crosshead speed tensile tests were conducted at the temperatures ranging from 375 to 470 °C using INSTRON 5848 micro-tester. The failed specimens were subjected to scanning electron microscopic (SEM) examinations. Further, the specimens deformed to failure at 450 °C and 1×10^{-2} s^{-1} were mounted, mechanically polished for OM and SEM examinations. The local true strain of deformed specimens were estimated by $\varepsilon = \ln(A_0/A_i)$, where A_0 is the original sectional area of the gage region and A_i is the sectional area of section i in a deformed specimens.

Results

Microstructural characteristics

Figure 1 shows the optical micrographs of the cast and FSP 7075Al samples. The as-cast microstructure was characterized by coarse grains and coarse second-phase particles at the grain boundaries, in particular at the triple junctions (Fig. 1a). After the homogenization treatment, most of the second-phase particles disappeared and the grains were somewhat coarsened (Fig. 1b).

After FSP, both the grains and the second-phase particles were significantly refined (Fig. 1c, d). The average grain sizes of the D-FSP and H-FSP samples were estimated to be ~3.2 and 2.5 μm, respectively. The second-phase particles in the H-FSP sample were fine and randomly distributed both within the grain interiors and at the grain boundaries (Fig. 1d). However, the second-phase particles in the D-FSP sample were comparatively large and tended to be distributed at the grain boundaries (Fig. 1c).

Superplastic behavior

Figure 2 shows the variation of superplastic elongation with the initial strain rate at different testing temperatures for the FSP samples. For the D-FSP sample, both the optimum strain rate for superplasticity and the maximum elongation increased with increasing the temperature. At

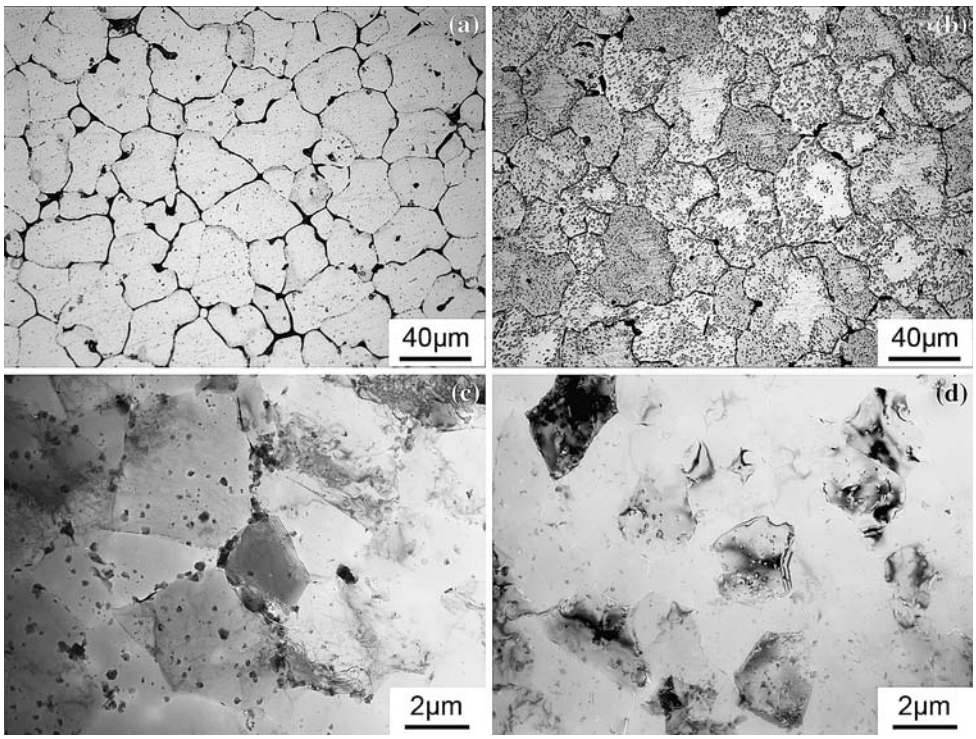

Fig. 1 Optical macrograph of 7075Al casting under **a** as-cast and **b** homogenized conditions, TEM micrographs showing grain structures of **c** D-FSP sample and **d** H-FSP sample

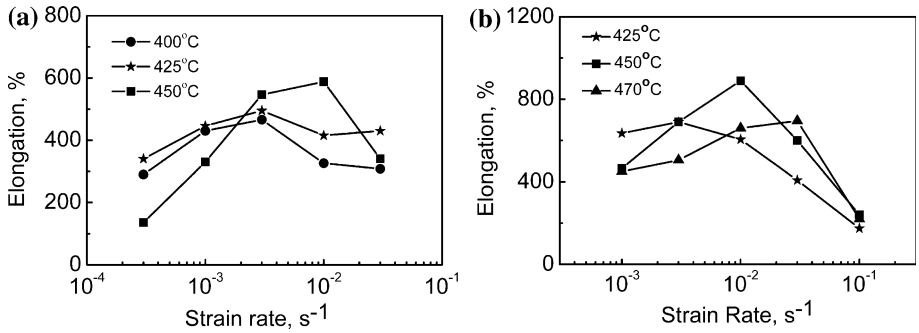

Fig. 2 Variation of elongation with initial strain rate at various testing temperatures for **a** D-FSP sample and **b** H-FSP sample

450 °C, the optimum strain rate for maximum elongation increased to a high train rate of 1×10^{-2} s^{-1}, and the largest elongation of 588% was achieved at 450 °C and 1×10^{-2} s^{-1}. At a constant strain rate of 1×10^{-2} s^{-1}, the superplasticity of the D-FSP sample increased with increasing testing temperature from 375 to 450 °C, however, above 450 °C, the superplastic ductility decreased rapidly and an elongation of 170% was observed at 470 °C (Fig. 3). For the H-FSP sample, the optimum strain rate for superplasticity was observed to be 1×10^{-2} s^{-1}. The largest elongation of 890% was achieved at 450 °C and 1×10^{-2} s^{-1}. Above 450 °C, the superplasticity of the H-FSP sample decreased with increasing the testing temperature (Fig. 3). Increasing the temperature to 470 °C, the optimum strain rate for maximum elongation was shifted to 3×10^{-2} s^{-1}, but the elongation was lower than that obtained at 450 °C and 1×10^{-2} s^{-1} (Fig. 2b).

Figure 4 shows the variation of flow stress (at true strain of 0.1) with initial strain rate for the FSP 7075Al samples.

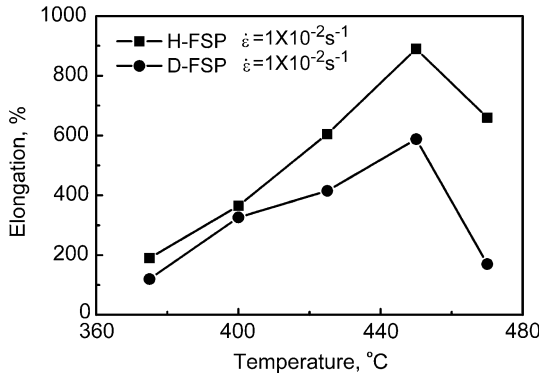

Fig. 3 Variation of elongation with testing temperature at initial strain rates of 1×10^{-2} s^{-1} for D-FSP and H-FSP samples

The flow stress increased with increasing the strain rate and decreasing the testing temperature. Strain-rate sensitivity (m) of $\sim$0.5 was observed under the investigated strain rate and temperature ranges for both D-FSP and H-FSP samples.

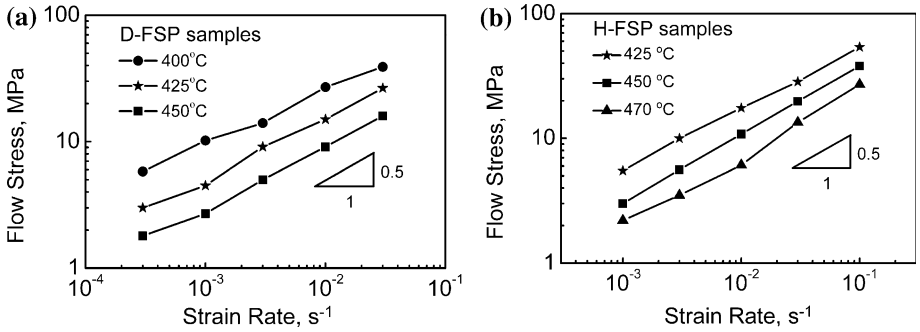

Fig. 4 Variation in flow stress with initial strain rate at various testing temperatures for **a** D-FSP sample and **b** H-FSP sample

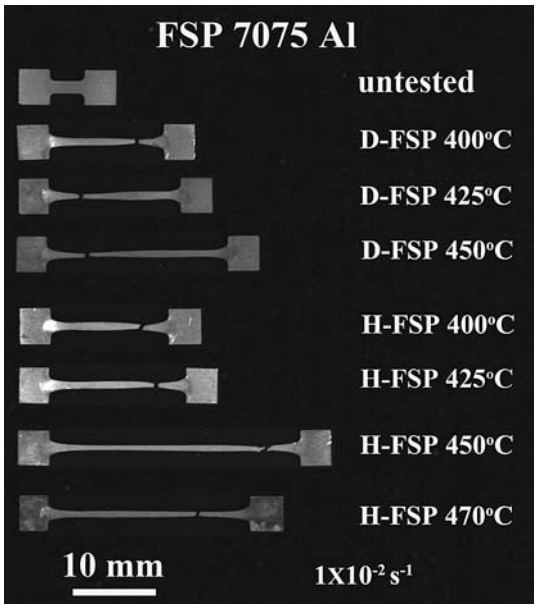

Fig. 5 Specimens of FSP cast 7075Al alloys tested at 1×10^{-2} s^{-1} with various temperatures

Figure 5 shows the failed tensile specimens deformed at a constant initial stain rate of 1×10^{-2} s^{-1} for different testing temperatures. All the specimens showed relatively uniform elongation, characteristic of superplastic flow.

Figure 6 shows the topography of the D-FSP and H-FSP samples deformed to failure at 450 °C and 1×10^{-2} s^{-1}. Grain boundary sliding was distinctly seen on the surfaces of two deformed specimens.

Cavitation

Figure 7 shows the microstructures near the fracture tips for the two FSP specimens deformed at 450 °C and 1×10^{-2} s^{-1}. The two specimens exhibited typical cavitation failure in which fracture occurred through cavity interlinkage without the development of visible necking.

Figure 8 shows the effect of true strain on the cavitation of the two FSP samples deformed at 450 °C and 1×10^{-2} s^{-1}. Similar observations were made in the two samples. At a lower true strain of 1.2–1.3, low densities of small cavities were distinctly detected in the two samples (Fig. 8a, b). Increasing the true strain to 1.5–1.6 resulted in the growth of the cavities and the formation of more new cavities, thereby increasing the density and volume of cavities (Fig. 8c, d). At a higher strain of 1.8–2.0, the growth, coalescence, and linkage of cavities became increasingly evident, resulting in an increase in the cavity volume (Fig. 8e, f).

Figure 9 shows the backscattered electron images of the FSP samples deformed at 450 °C and an initial strain rate

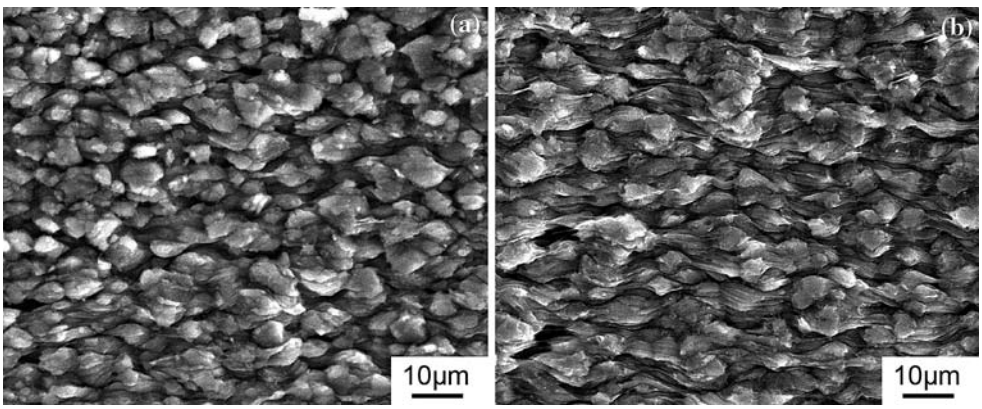

Fig. 6 SEM micrographs showing surface topographies of failed tensile specimens deformed at 450 °C and 1×10^{-2} s^{-1}: **a** D-FSP and **b** H-FSP

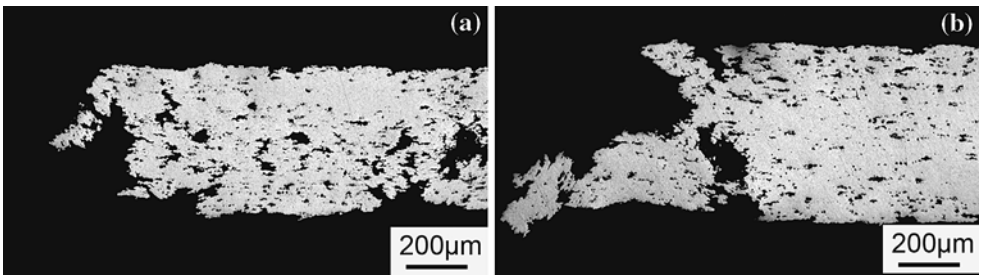

Fig. 7 Appearance of fracture tips for specimens tested at 450 °C and an initial strain rate of 1×10^{-2} s^{-1}: **a** D-FSP and **b** H-FSP

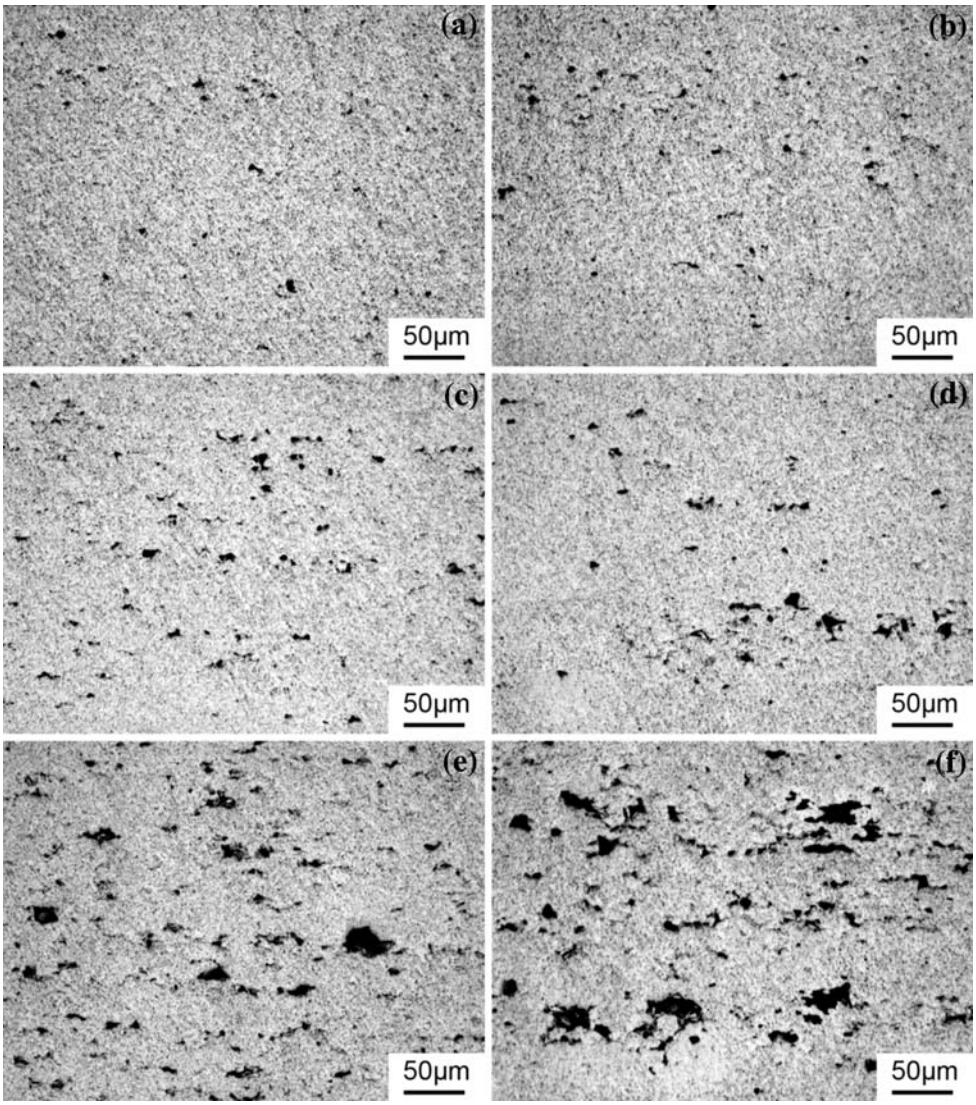

Fig. 8 Optical micrographs showing cavitation of D-FSP sample deformed to a true strain of **a** 1.2, **c** 1.5, and **e** 1.8, and H-FSP sample deformed to a true strain of **b** 1.3, **d** 1.6, and **f** 2.0 (450 °C and 1×10^{-2} s^{-1}, the tensile axes are horizontal)

of 1×10^{-2} s^{-1} to a true strain of $\sim$1.8. It is clearly showed that the formation of cavities was associated with the coarse particles and the triple junctions of the grains. It is noted that the D-FSP sample contained a higher population density of the particles and cavities than the H-FSP sample.

Discussion

Microstructural characteristics

The cast 7075Al was characterized by the coarse grains and coarse second-phase particles distributed at the grain triple

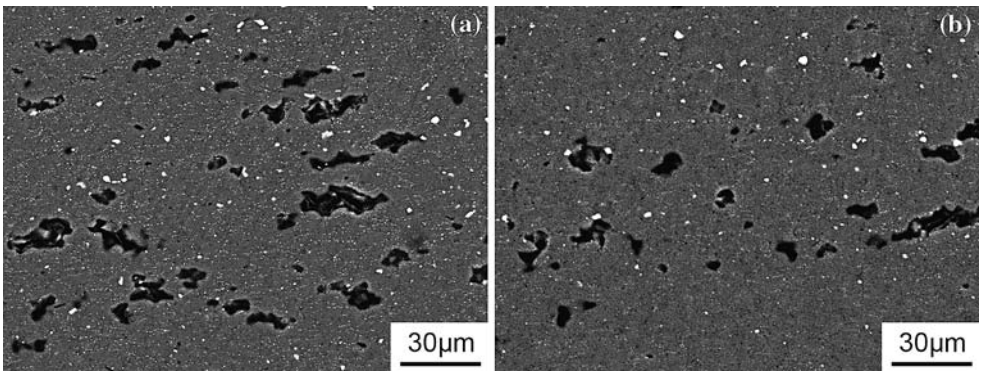

Fig. 9 SEM micrographs showing cavity formation at large particles and grain triple junctions in samples deformed at 450 °C and 1×10^{-2} s^{-1} to a true strain of ~1.8 (tensile axis is horizontal): **a** D-FSP and **b** H-FSP

junctions (Fig. 1a). During the homogenization treatment, most of the coarse particles dissolved into the aluminum matrix, resulting in the fundamental elimination of the coarse particles (Fig. 1b). FSP resulted in the generation of the fine and equiaxed grains due to the occurrence of the dynamic recrystallization and the breakup of the coarse particles due to the intense stirring effect of the threaded pin (Fig. 1c, d). It is noted that the D-FSP sample had coarser second-phase particles and grains than the H-FSP sample.

The previous studies were mainly focused on the effects of the processing parameters on microstructural evolution, material flow pattern, and mechanical properties [14–20]. Only a small number of studies involved in the effect of the raw material conditions on resultant microstructure in the SZ [21, 22]. The present study indicates that the coarse particles in the raw material affected the microstructural refinement and homogenization of FSP aluminum samples. A homogenized starting microstructure is beneficial to obtaining the fine-grained structure with the finer particles. The second-phase particles in 7075Al alloy were previously identified to be Cr-bearing dispersoids and $MgZn_2$-type precipitates [23]. Large particles at the grain boundaries tend to promote cavity development during superplastic deformation [8, 24]. This will be discussed in Sect. Cavity formation.

Superplasticity

Figure 2 shows that the simple application of FSP induced high strain rate superplasticity in the cast 7075Al. Similarly, FSP converted a non-superplastic cast A356 to a superplastic one [11]. This demonstrates that FSP is a very effective processing technique to induce superplasticity in the cast aluminum alloys. Therefore, it is a feasible method to fabricate fine-grained superplastic high-strength commercial aluminum alloys from the as-cast structure directly via FSP. This will shorten the fabrication period of

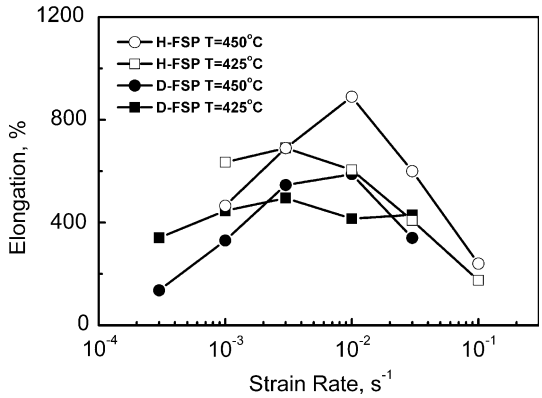

Fig. 10 Comparison of superplastic ductility between D-FSP and H-FSP samples as a function of strain rate

fine-grained superplastic materials and reduce the fabrication cost. However, two FSP 7075Al samples with different initial structures exhibited different superplastic properties. As shown in Figs. 3 and 10, the H-FSP sample exhibits better superplasticity than the D-FSP sample. This indicates that the homogenization treatment prior to FSP improved the superplastic properties of FSP 7075Al casting. This is attributed to finer and more uniformly distributed particles in the H-FSP sample. As will be discussed, the finer particles tend to reduce the cavitation in superplastically deformed samples.

In a previous study [7], it was reported that FSP resulted in the generation of superplasticity of more than 1250% at 1×10^{-2} s^{-1} and 480 °C in the rolled 7075Al plates. By comparison, the optimum superplastic deformation temperature was observed to be 450 °C in the present FSP 7075Al cast samples. This is attributed to the decrease in the grain size. However, the FSP cast samples exhibited a lower ductility than the previous FSP 7075 rolled plates, though the FSP cast samples had a smaller grain size [7]. This indicates that a single-pass FSP on the as-cast 7075Al could not produce the best superplasticity. This might be attributed to the following factors. First, the fine-grained

structure obtained by FSP in the casting was not very homogeneous with relatively large second-phase particles at the grain boundaries. Second, the ratio of high-angle grain boundaries in the present FSP samples might be lower than that in the FSP 7075 rolled plates [7, 8]. More microstructural examinations are needed to reveal the origin of lower superplasticity in the FSP cast 7075Al samples. Furthermore, more FSP attempts are conducted to optimize the FSP parameters to produce better superplasticity in the cast 7075Al samples.

For SPF of most industrial components, usually, a superplasticity of 200%–300% can meet the SPF requirement. Therefore, although FSP produced a lower superplasticity in the cast 7075Al samples than that in the rolled samples, the obtained superplastic values are enough for SPF.

Deformation mechanism

For a fine-grained structure, the grain boundary sliding (GBS) with a strain-rate sensitivity of 0.5 is expected to be the dominant superplastic deformation mechanism. For the D-FSP and H-FSP samples, a strain-rate sensitivity of $\sim$0.5 was observed in the strain rate range of 3×10^{-4}–1×10^{-1} s^{-1} for the investigated temperatures (Fig. 4). This implies that the main mechanism for superplastic deformation of the FSP 7075Al samples is the GBS. Additionally, the GBS was further verified by SEM examinations on the surfaces of the deformed specimens (Fig. 6). This behavior is similar to that observed in the previous FSP 7075Al rolled plates [7], in which constant strain-rate sensitivities of $\sim$0.5 were observed throughout the strain-rate range of 1×10^{-3}–1×10^{-1} s^{-1} in the temperature range of 470–490 °C.

The constitutive relationship for superplasticity in fine-grained aluminum alloys can be expressed as [25],

$$\dot{\varepsilon} = 40\frac{D_0 Eb}{kT}\exp\left(\frac{-84000}{RT}\right)\left(\frac{b}{d}\right)^2\left(\frac{\sigma-\sigma_o}{E}\right)^2 \quad (1)$$

where $\dot{\varepsilon}$ is the strain rate, D_0 is the pre-exponential constant for diffusivity, E is Young's modulus, b is Burger's vector, k is Boltzmann's constant, T is the absolute temperature, R is the gas constant, d is the grain size, σ is the applied stress, and σ_o is the threshold stress.

To further elucidate the superplastic deformation mechanism in the FSP 7075Al samples, superplastic data from the two FSP samples are plotted in Fig. 11 as $((\dot{\varepsilon}kTd^2/(D_gEb^3)))$ versus s/E. For comparison, a dashed line predicted by Eq. 1 was also included. Four important observations can be made from this plot. First, the temperature dependence of superplastic flow for both FSP samples is similar to the activation energy for aluminum

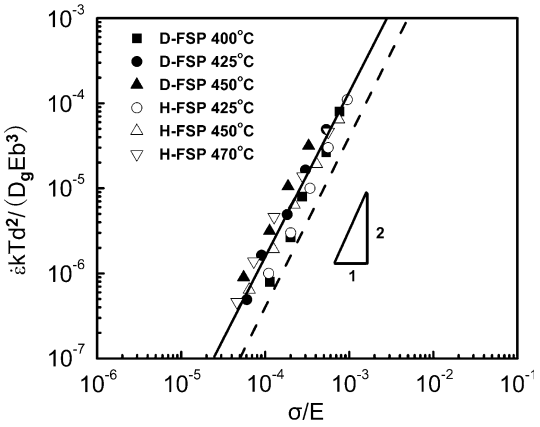

Fig. 11 Variation of $(\dot{\varepsilon}kTd^2/(D_gEb^3))$ with normalized stress for FSP 7075Al alloys

grain boundary self-diffusion. Second, the data of the two samples fit into a single straight line with a slope of 2, showing that the stress dependence of superplastic flow is approximately $2(\dot{\varepsilon} \propto \sigma^2)$. Third, the data of the two FSP samples merge after the strain rates are normalized by the square of the grain sizes. This shows an inverse grain size dependence of 2 for superplastic flow. Fourth, the dimensionless constant that fit the data for the FSP samples was larger than that found in Eq. 1. A stress exponent of 2, an inverse grain size dependence of 2, and activation energy close to that for grain boundary self-diffusion are associated with the grain boundary sliding models of Mukherjee [26] and Ball and Hutchinson [27]. Thus, Fig. 11 shows that grain boundary sliding is the main superplastic deformation mechanism for the present FSP 7075Al samples.

In this analysis, superplastic data of the two FSP samples can be described by

$$\dot{\varepsilon} = 187\frac{D_0 Eb}{kT}\exp\left(\frac{-84000}{RT}\right)\left(\frac{b}{d}\right)^2\left(\frac{\sigma-\sigma_o}{E}\right)^2 \quad (2)$$

The dimensionless constant in Eq. 2 is larger than that in Eq. 1. Ma et al. [7] examined the superplastic data of FSP 7075Al rolled plates with two different grain sizes of 3.8 and 7.5 μm, and a dimensionless constant of 790 was observed by normalizing the superplastic data. Similarly, Johannes and Mishra [10] obtained a much higher constant of 1396 in a FSP 7075Al with a grain size of 4.7 μm. The higher constants than 40 demonstrate that the flow stresses of the FSP alloys were lower than that predicted by Eq. 1 at a given temperature, grain size, and stain rate. This was attributed to higher ratio of the high-angle grain boundaries in the FSP alloys that facilitate the GBS during the superplastic deformation [7]. The lower constant observed in the FSP cast 7075Al samples suggested that the number fraction of high-angle grain boundaries in the FSP cast

7075Al samples was lower than that in the FSP rolled plates. This implies that the non-homogeneous as-cast structure with the coarse second-phase particles and coarse aluminum dendrites decreased the material flow ability during FSP, thereby producing a microstructure with relatively large particles and reduced number fraction of the high-angle grain boundaries.

Cavity formation

It is well documented that when the GBS is the dominant mechanism of superplastic deformation in the superplastic materials, the sliding needs to be accommodated by other mechanisms, for example, grain-boundary migration, diffusion flow, or dislocation slip. When the GBS cannot be well accommodated, stress concentration at certain sites, such as the grain triple junctions, second-phase particles, and boundary ledges, etc. may cause the development of cavitation at the sites [8, 28, 29]. In particular, many investigators have noted that the majority of cavities were associated with second-phase particles [23, 30–32]. For the particles at the grain boundaries, as in most superplastic alloys, their non-deformability and the additional interfacial energy aid the stability of the cavity. With the large particles, accommodation processes of GBS become inadequate to suppress cavity nucleation. Furthermore, grain growth occurring during superplastic flow that leads to flow hardening can also cause additional cavity nucleation at smaller particles in a continuous manner [33].

Bae et al. [23] reported that most cavities were observed at the interface between particles and the matrix, and grew initially along the interface. However, Ma et al. [8] pointed out that for the FSP 7075Al rolled plates, the cavitation was more often observed to develop at the grain triple junctions due to the fine and relatively uniformly distributed precipitates in the FSP alloys. For the present FSP 7075Al samples, it appeared that the cavities initiated at both the particles and the grain triple junctions (Fig. 9). New cavities formed continuously during deformation, and these cavities grew and interlinked to large cavities as the strain increased (Fig. 8). The D-FSP sample contained a higher population density of particles, in particular larger particles, than the H-FSP sample (Figs. 1 and 9). These particles provided more cavity nucleation sites during superplastic deformation. Therefore, the D-FSP sample exhibited more and larger cavities than the H-FSP sample at a constant true strain of $\sim$1.8, and therefore exhibited a lower superplasticity.

Conclusions

1. A single-pass FSP converted the as-cast structure of 7075Al sample to the fine-grained structure with a grain size of 2.5–3.2 μm successfully. A pre-homogenization prior to FSP was beneficial to producing a more uniform microstructure with smaller particles and grains.
2. The FSP 7075Al samples exhibited maximum superplasticity at a high strain rate of 1×10^{-2} s^{-1} and 450 °C. Pre-homogenization increased the superplastic ductility significantly and the largest elongation of 890% was achieved at 450 °C and 1×10^{-2} s^{-1} in the FSP sample with a pre-homogenization.
3. Cavity nucleation was associated with the coarse particles or the grain triple junctions in the FSP 7075Al samples. The FSP sample with a pre-homogenization had less and smaller cavities due to reduced particle size, thereby producing a better superplasticity.
4. The analyses on the superplastic data indicate that GBS is the primary superplastic deformation mechanism for the FSP 7075Al samples, which was verified by SEM examinations on the surfaces of deformed specimens. However, the dimensionless constant was lower than that observed in FSP 7075Al rolled plates.

Acknowledgements The author gratefully acknowledges the support of (a) the National Outstanding Young Scientist Foundation with Grant No. 50525103, (b) the National Basic Research Program of China under Grant No. 2006CB605205, (c) the National High-tech Research Program under Grant No. 2006AA03Z111, and (d) the Hundred Talents Program of Chinese Academy of Sciences.

References

1. Barnes AJ (1994) Mater Sci Forum 170–172:701
2. Pilling J, Ridley N (1989) Superplasticity in crystalline solids. The Institute of Metals, London, p 214
3. Thomas WM, Nicholas ED, Needham JC, Murch MG, Templesmith P, Dawes CJ (1991) GB Patent Application No. 9125978.8
4. Mishra RS, Mahoney MW, McFadden SX, Mara NA, Mukherjee AK (2000) Scripta Mater 42:163
5. Mishra RS, Ma ZY (2005) Mater Sci Eng R50:1
6. Berbon PB, Bingel WH, Mishra RS, Bampton CC, Mahoney MW (2001) Scripta Mater 44:61
7. Ma ZY, Mishra RS, Mahoney MW (2002) Acta Mater 50:4419
8. Ma ZY, Mishra RS (2003) Acta Mater 51:3551
9. Dutta A, Charit L, Johannes LB, Mishra RS (2005) Mater Sci Eng A 395:173
10. Johannes LB, Mishra RS (2007) Mater Sci Eng A 464:255
11. Ma ZY, Mishra RS, Mahoney MW (2004) Scripta Mater 50:931
12. Charit I, Mishra RS (2005) Acta Mater 53:4211
13. Johannes LB, Charit I, Mishra RS, Verma R (2007) Mater Sci Eng A 464:351
14. Sato YS, Urata M, Kokawa H, Ikeda K, Enomoto M (2001) Scripta Mater 45:109
15. Benavides S, Li Y, Murr LE, Brown D, Mcclure JC (1999) Scripta Mater 41:809
16. Liu G, Murr LE, Niou CS, Mcclure JC, Vega FR (1997) Scripta Mater 37:355
17. Seidel TU, Reynolds AP (2001) Metall Mater Trans 32A:2879

18. Li Y, Murr LE, Mcclure JC (1999) Scripta Mater 40:1041
19. Liu HJ, Fujii H, Maeda M, Nogi K (2004) J Mater Sci Technol 20:103
20. Liu FC, Ma ZY (2008) Scripta Mater 58:667
21. Sato YS, Urata M, Kokawa H (2002) Metall Mater Trans 33A:625
22. Chen YC, Liu HJ, Feng JC (2006) Mater Sci Eng A 420:21
23. Mahoney MW, Rhodes CG, Fiulintoff JG, Spruling RA, Bingel WH (1998) Metall Mater Trans 29A:1955
24. Bae DH, Ghosh AK (2002) Acta Mater 50:511
25. Mishra RS, Bieler TR, Mukherjee AK (1995) Acta Metall Mater 43:877
26. Arieli A, Mukherjee AK (1980) Mater Sci Eng 45:61
27. Ball A, Hutchinson MW (1969) Metal Sci J 3:1
28. Shin DH, Park KT (1999) Mater Sci Eng A 268:55
29. Chokshi AH (1997) Mater Sci Forum 89:233
30. Park KT, Myung SH, Shin DH, Lee CS (2004) Mater Sci Eng A 371:178
31. Pandey MC, Wadsworth J, Mukherjee AK (1988) J Mater Sci 23:3509. doi:10.1007/BF00540488
32. Yasuda HY, Hiraga K (1997) Mater Sci Eng A 234:343
33. Ghosh AK (1982) In: Hanson H, Horsewell A, Leffers T, Lilholt H (eds) Deformation of polycrystals: mechanisms and microstructures. Riso National Laboratory, Roskilde, Denmark, p 27